The Hexahistidine Motif of Host-Defense Protein Human Calprotectin Contributes to Zinc Withholding and Its Functional Versatility

HHS Public Access

Author manuscript

J Am Chem Soc. Author manuscript; available in PMC 2016 September 27.

Published in final edited form as:

J Am Chem Soc. 2016 September 21; 138(37): 12243–12251. doi:10.1021/jacs.6b06845.

The Hexahistidine Motif of Host-Defense Protein Human Calprotectin Contributes to Zinc Withholding and Its Functional Versatility

Toshiki G. Nakashige[1], **Jules R. Stephan**[1], **Lisa S. Cunden**[1], **Megan Brunjes Brophy**[1], **Andrew J. Wommack**[1], **Brenna C. Keegan**[2], **Jason M. Shearer**[2], and **Elizabeth M. Nolan**[1,*]

[1]Department of Chemistry, Massachusetts Institute of Technology, Cambridge, MA 02139

[2]Department of Chemistry, University of Nevada, Reno, NV 89503

Abstract

Human calprotectin (CP, S100A8/S100A9 oligomer, MRP-8/MRP-14 oligomer) is an abundant host-defense protein that is involved in the metal-withholding innate immune response. CP coordinates a variety of divalent first-row transition metal ions, which is implicated in its antimicrobial function, and its ability to sequester nutrient Zn(II) ions from microbial pathogens has been recognized for over two decades. CP has two distinct transition-metal-binding sites formed at the S100A8/S100A9 dimer interface, including a histidine-rich site composed of S100A8 residues His17 and His27 and S100A9 residues His91 and His95. In this study, we report that CP binds Zn(II) at this site using a hexahistidine motif, completed by His103 and His105 of the S100A9 C-terminal tail and previously identified as the high-affinity Mn(II) and Fe(II) coordination site. Zn(II) binding at this unique site shields the S100A9 C-terminal tail from proteolytic degradation by proteinase K. X-ray absorption spectroscopy and Zn(II) competition titrations support the formation of a Zn(II)-His_6 motif. Microbial growth studies indicate that the hexahistidine motif is important for preventing microbial Zn(II) acquisition from CP by the probiotic *Lactobacillus plantarum* and the opportunistic human pathogen *Candida albicans*. The Zn(II)-His_6 site of CP expands the known biological coordination chemistry of Zn(II) and provides new insight into how the human innate immune system starves microbes of essential metal nutrients.

Graphical Abstract

*Corresponding author: lnolan@mit.edu, Phone: 617-452-2495, Fax: 617-324-0505.

The authors declare no competing financial interests.

Associated Content

Supporting Information. Complete experimental methods and additional data. This material is available free of charge via the Internet at http://pubs.acs.org.

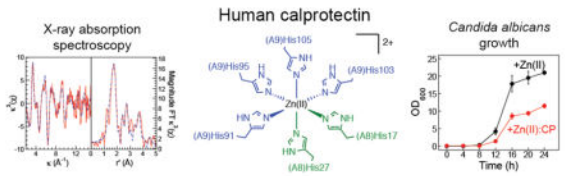

Introduction

Zinc is an essential nutrient for all organisms,[1] and the interplay between host and microbe for this metal is an important component of innate immunity and microbial pathogenesis.[2–5] The host innate immune system deploys Zn(II)-sequestering proteins at sites of infection to reduce the bioavailable Zn(II) pool.[2–4] Human calprotectin (CP, S100A8/S100A9 oligomer, MRP-8/MRP-14 oligomer) is a Ca(II)-dependent host-defense protein that contributes to the metal-withholding response by chelating extracellular Zn(II)[6–8] as well as Mn(II)[9] and Fe(II).[10]

The CP heterodimer exhibits two transition-metal-binding sites at the S100A8/S100A9 interface (Figure 1).[11–17] Site 1 is a His_3Asp motif comprising (A8)His83, (A8)His87, (A9)His20, and (A9)Asp30. This site binds Zn(II) with high affinity,[12,13] and exhibits markedly lower affinities for Mn(II)[14,15,17] and Fe(II).[10] Site 2 is described as a His_4 or His_6 motif. This site was first identified in the X-ray structure of Ca(II)-bound CP by four His residues that are located at the S100A8/S100A9 interface, (A8)His17, (A8)His27, (A9)His91, and (A9)His95.[11] Subsequent investigations revealed that (A9)His103 and (A9)His105, located in the S100A9 C-terminal tail, complete a His_6 coordination sphere for Mn(II)[15–17] and Fe(II)[10] that is unprecedented in biological systems. Site 2 also coordinates Zn(II) with high affinity.[12,13] In agreement with the Irving-Williams series,[18] Zn(II) binding is thermodynamically favored over Mn(II) and Fe(II);[10,14] however, whether site 2 employs the His_4 or His_6 motif for Zn(II) coordination remains unclear.

In this work, we uncover new facets of the biological coordination chemistry of Zn(II) and the metal-sequestering function of CP. We establish that CP employs its unusual His_6 motif to entrap Zn(II) at site 2. To the best of our knowledge, CP provides the first example of a biological Zn(II)-His_6 coordination motif. Moreover, we show that this motif is essential for CP to use site 2 to deprive two microbial species of Zn(II). Our discovery is consistent with previous studies on the Mn(II) and Fe(II) coordination chemistry at this site[10,15–17] and indicates that this hexahistidine motif performs a versatile metal-scavenging function during the innate immune response.

Results and Discussion

Zn(II) Coordination at Site 2 Prevents Proteolysis by Proteinase K

In our reported metal-binding studies, we employed the S100A8(C42S)/S100A9(C3S) variant CP-Ser (Table 1) to avoid complications associated with cysteine-based oxidation of the protein.[13] The native Cys residues are distant from the metal-binding sites (Figure 1D), and CP-Ser displays comparable antibacterial activity to native CP.[13] During an exploratory

set of protease stability assays using CP variants that were monitored by analytical high performance liquid chromatography (HPLC), we observed that treatment of CP-Ser (+Ca) with proteinase K resulted in loss of the S100A8(C42S) and S100A9(C3S) peaks and formation of two new peaks with similar retention times to the full-length subunits (Figure 2A). Analysis of these new species by liquid chromatography-mass spectrometry (LC-MS) revealed that proteinase K selectively cleaves S100A8 after (A8)Glu89 and S100A9 after (A9)His104 (Table S4). These locations are near the His_3Asp and His_4/His_6 transition metal sites, respectively (Figure 1D). Incubation of CP-Ser (+Ca) with 1.0 equivalent of Mn(II), which fully occupies the His_6 site, resulted in protection of the S100A9 cleavage site only (Figures 2B, S5), whereas incubation of CP-Ser (+Ca) with 2.0 equivalents of Zn(II), which fully populate both sites 1 and 2, resulted in protection of both cleavage sites (Figure 2C, S6). We next examined the proteinase K susceptibility of variants that lack one or more His residues in the S100A9 C-terminal tail, H103A, H105A, and the double-mutation variant AHA (Figures 2B–C, S5–6; see Table 1 for nomenclature). These variants retain the ability to coordinate Mn(II) at site 2, albeit with an altered primary coordination sphere and lower affinity,[16,17] and based on prior work,[12] we reasoned that they coordinate Zn(II) as well (*vide infra*). When Mn(II) or Zn(II) was added to each of these variants, proteinase K cleaved the S100A9 subunit after (A9)H104. The H104A variant was also tested, and because the His_6 motif is conserved in this protein, proteolysis of the S100A9 subunit was not observed for Mn(II)- or Zn(II)-bound H104A (Figures 2B–C, S5–6). These foot-printing results showed that metal binding at site 1 (Zn) and site 2 (Mn, Zn) protects the CP scaffold from proteinase K, and that both (A9)His103 and (A9)His105 are required for metal-dependent protection of the S100A9 subunit. Thus, the Zn(II) data provided evidence for the involvement of residues (A9)His103 and (A9)His105 in Zn(II) coordination at site 2.

X-Ray Absorption Spectroscopy Supports a Hexahistidine Coordination Motif

We prepared a sample of the metal-binding site variant ΔHis_3Asp (Table 1) with substoichiometric Zn(II) and excess Ca(II) to interrogate Zn(II) bound at site 2 by using X-ray absorption spectroscopy (XAS). From an analysis of the X-ray absorption near-edge structure (XANES) region of the spectrum (Figure 3A), we can conclude that Zn(II) is not contained in a five- or four-coordinate ligand environment at site 2 and that the metal center is most likely six coordinate based on the large edge feature at 9665.9(1) eV.[19,20]

Furthermore, analysis of the extended X-ray absorption fine structure (EXAFS) region was most consistent with Zn(II) in a His_6 coordination environment (Figure 3). The best model yielded one shell containing four $Zn–N^{His}$ scatterers at 2.20 Å and one shell containing two $Zn–N^{His}$ scatterers at 2.08 Å. In addition to the model containing two short and four long scatterers, and alternative model was located that contains three short and three long $Zn–N^{His}$ scatterers with identical metric parameters. This model yielded slightly poorer fit statistics (ε^2 = 1.01 versus 0.98), but is a statistically valid model nonetheless. Alternative fits that contained fewer than six $Zn–N^{His}$ ligands yielded poor agreement with the experimental data or chemically unrealistic refinement parameters (i.e., negative σ^2 values) (Table S5).

To further evaluate the validity of these structural models, we performed a bond valence sum (BVS) analysis.[21–23] This empirical analysis compares the observed bond lengths of a metal center with a reference bond length. In an ideal case, the BVS value should equal the oxidation state of the metal ion (i.e., 2.00 for Zn(II)). It is therefore well suited for EXAFS results, where the coordination number is the least reliable refinement parameter. When employed to the above models, both analyses yielded a BVS value that is consistent with Zn(II). The model with four long and one short Zn–N^{His} scatterer afforded BVS = 1.85, and the model containing three short and three long Zn–N^{His} scatterers afforded BVS = 1.95. From this analysis, the latter model may be considered a better fit to the data; however, both models are considered to be valid structural models for this site.

The Zn–N^{His} bond lengths determined from the two models are consistent with the reported Zn–N^{His} bond lengths in protein crystal structures deposited in the Protein Data Bank,[24] which are typically in the range of 2.00–2.30 Å (Table S6). Moreover, X-ray structures of small-molecule hexaimidazole Zn(II) complexes deposited in the Cambridge Structural Database[25] have Zn–N bond lengths in the range of 2.18–2.20 Å.[26,27]

Taken together with the proteinase K foot-printing study and the results presented below, we conclude that Zn(II) bound at site 2 is in a 6-coordinate geometry provided by the His_6 motif (Figure 4). To the best of our knowledge, no protein with a Zn(II)-His_6 site has been reported to date. Although Zn(II) is a d^{10} metal ion that adopts a variety of coordination numbers and geometries,[28] only ≈ 5% of Zn(II) proteins in the Protein Data Bank exhibit a 6-coordinate Zn(II) center.[29] No deposited protein structure contains >4 His residues bound to a single Zn(II) ion, and there is only one example of a 6-coordinate Zn(II) ion containing 4 His residues. This protein, a polyketide cyclase from *Streptomyces resistomycificus*, exhibits a N_4O_2 coordination sphere where two water molecules bind Zn(II) *cis* to one another to complete the 6-coordinate geometry.[30] Because CP has a unique Zn(II)-binding site, we sought to further investigate the contribution of the hexahistidine motif to the affinity CP for this metal ion at site 2 and its Zn(II)-sequestering function against microorganisms.

The C-Terminal Tail Enhances the Zn(II) Affinity at Site 2

CP-Ser employs sites 1 and 2 for coordinating two equivalents of Zn(II) with high affinity in both the absence and presence of Ca(II).[12,13] Moreover, the Zn(II) affinities of sites 1 and 2 depend on Ca(II), and we observed that CP-Ser (+Ca) could outcompete the fluorescent Zn(II) sensor ZP4 (apparent $K_{d,Zn}$ = 0.65 nM, pH 7.0)[31] for Zn(II).[13] As a result, these ZP4 competitions only provided upper limits to the apparent K_d values of CP-Ser (+Ca) of 10 pM and 240 pM.[13] We sought to build upon this preliminary work and the experiments described above that implicated (A9)His103 and (A9)His105 in Zn(II) binding and to evaluate how His103 and His105 contribute to the Zn(II) affinity of CP-Ser. We performed Zn(II) competition experiments with CP-Ser variants that lack one or more of the His residues of the C-terminal tail. First, we confirmed that the AAA variant that lacks the three His residues of the S100A9 C-terminal tail (Table 1) coordinates two equivalents of Zn(II) by conducting competition titrations with the colorimetric Zn(II) chelator Zincon ($K_{d,Zn}$ μ 10 μM)[32,33] (Figures 5A, S8). Next, we performed Zn(II) competition titrations with ZP4 and

AAA. In the presence of excess Ca(II), the titration curve we obtained for AAA was nearly identical to that of CP-Ser (Figure 5B), indicating that high-affinity Zn(II) binding is retained in the absence of (A9)His103 and (A9)His105. These results are in agreement with a prior study that reported stoichiometric Zn(II) binding for the CP-Ser variants HN Tail (AAA analogue with His to Asn mutations at positions 103–105) and ΔTail (a truncation variant that lacks residues 103–114) by isothermal titration calorimetry.[12]

To perform experiments with a higher affinity competitor and thereby probe for differences in the Zn(II)-binding properties of Ca(II)-bound CP-Ser and AAA, we synthesized and utilized the Ca(II)-insensitive turn-on fluorescent Zn(II) sensor HNBO-DPA (apparent $K_{d,Zn}$ = 12 pM, pH 7.0) (Figure S9).[34] We titrated Zn(II) into a solution containing 5 μM CP-Ser, 2 μM HNBO-DPA, and 250 μM Ca(II), and observed negligible fluorescence enhancement from HNBO-DPA until >10 μM Zn(II) was added. Thus, CP-Ser outcompeted HNBO-DPA for ≈ 2 equivalents of Zn(II) under these conditions (Figures 5C–D, S10). This titration indicates that CP-Ser (+Ca) binds Zn(II) with sub-picomolar affinity at both sites. The data could be fit with the apparent dissociation constant (K_d) values K_{d1} = 90 fM and K_{d2} = 0.9 pM (black line, Figure 5D; Supporting Information), which we consider to be approximate upper limits. These values are three to four orders of magnitude lower than the upper limits for Zn(II) binding by CP-Ser (+Ca) obtained with ZP4.

In contrast, titrations with tail variants afforded competition between the protein and HNBO-DPA, even at <5 μM Zn(II) (Figures 5C, S10). These results indicate that site 1 cannot outcompete HNBO-DPA for Zn(II) in the absence of the intact His_6 motif at site 2. Fitting the AAA titration afforded $K_{d1,Zn}$ = 4.0 ± 0.8 pM and $K_{d2,Zn}$ = 22 ± 3 pM (red line, Figure 5D). These data provide the first suggestion of allostery between sites 1 and 2 of CP. In prior work, we established that Ca(II) binding to the EF-hand domains enhances the affinity of CP for transition metals,[10,13,14] and the possibility of cooperativity between the transition metal sites adds another layer of complexity to the coordination chemistry of this host-defense protein. Further evaluating this possibility and determining whether the Mn(II) or Fe(II) affinity at site 2 is influenced by the presence of Zn(II) or another metal ion at site 1 are avenues for future investigation.

At present, only upper limits for the Mn(II), Fe(II) and Zn(II) apparent K_d values of Ca(II)-bound CP-Ser are available. Stoichiometric binding is observed in direct metal-ion titrations,[12,14,15] and in the presence of Ca(II), the protein has outcompeted the small-molecule chelators identified and employed to date.[10,13,14] As a result, the upper limits to the K_d values that have been reported depend on the metal affinity of the competitor, and consequently, a direct comparison of these values does not necessarily reflect relative affinities of CP for different metals. The data obtained from early Zn(II) competition experiments with the nanomolar competitor ZP4 (where an upper limit of $K_{d1,Zn}$ ≤10 pM was able to be fit)[13] and those from Fe(II) competition experiments with the picomolar competitor Zinpyr-1 (ZP1) (where an upper limit of $K_{d,Fe}$ < 2.2 pM was established due to complete outcompetition) illustrate this point because metal substitution experiments established that site 2 (±Ca) has a thermodynamic preference for Zn(II) over Fe(II) or Mn(II) (i.e., $K_{d,Zn} < K_{d,Fe} < K_{d,Mn}$). The inherent limitations associated with different metal-ion competitors must therefore be carefully considered in the context of comparing the metal

affinities of CP. The current Zn(II) competition data provide upper limits in the femtomolar and sub-picomolar range (*vide supra*). Moreover, in our initial studies of Zn(II) binding, we attributed site 1 to have higher affinity for Zn(II) than site 2 on the basis of Zn(II) competition titrations performed in the absence of Ca(II).[13] Given subsequent insights about the coordination chemistry of site 2 and the fact that the site 2 variants examined here are not able to outcompete HNBO-DPA for one equivalent of Zn(II), we question whether these relative affinities remain the same in the presence of Ca(II). We have decided not to make site-specific K_d assignments from the fittings presented in this work. Indeed, continued efforts to identify new probes are required to build upon the current results and further ascertain the Zn(II) affinities for this metal-chelating protein.

Metal Analysis of Bacterial Growth Media Treated with CP Tail Variants

Because the Zn(II) competition titrations indicated that both CP-Ser and AAA bind 2 equivalents of Zn(II) with high affinity, we questioned whether the native His_6 site is essential for Zn(II) sequestration at site 2. To probe site 2 in isolation, we prepared and characterized four new CP-Ser variants based on ΔHis_3Asp that lack residues in the S100A9 tail: ΔHis_3Asp(H103A), ΔHis_3Asp(H104A), ΔHis_3Asp(H105A), and ΔHis_3Asp-AAA (Table 1, Figures S1–S4). Our prior work indicated that the ability of CP-Ser to inhibit *Lactobacillus plantarum* growth results from Zn(II) deprivation,[10] and we therefore selected *L. plantarum* as a model organism to evaluate the activity of these variants. This probiotic bacterium has a notably high metabolic requirement for Mn,[35] and Lactobacilli have also been reported to accumulate Zn during growth in nutrient-rich media.[36,37] The *L. plantarum* growth medium employed in our studies (Tris:MRS) contains ≈ 10 μM Zn, ≈ 100 μM Mn, ≈ 5 μM Fe, and ≈ 2 mM Ca (Figures 6, S11; Table S8). First, we compared the metal-depletion profiles of CP-Ser, AAA, ΔHis_3Asp, and ΔHis_3Asp-AAA for this medium. Treatment with these proteins (0–250 μg/mL, which corresponds to 0–11 μM heterodimer) reduced the levels of Zn in a concentration-dependent manner, and those of other metals showed negligible change (Figures 6, S11; Tables S9–S20). The AAA and ΔHis_3Asp-AAA variants depleted Zn more readily than CP-Ser and ΔHis_3Asp, respectively. For example, treatment with 250 μg/mL CP-Ser resulted in 11-fold Zn depletion, whereas AAA decreased Zn levels >100-fold. Our prior studies demonstrated that (A9)His103 and (A9)His105 are required for CP to sequester labile Mn(II) and Fe(II),[10,16] and we previously argued that the His_6 motif will retain the metal ion that binds there first.[10] Because of the high Mn content in Tris:MRS (≥10-fold excess over Zn or Fe), we reason that Mn(II) will predominantly occupy the His_6 site; however, without (A9)His103 and/or (A9)His105, metal ions will exchange more readily at this site. As a result, AAA and ΔHis_3Asp-AAA more selectively deplete Zn(II), which is thermodynamically favored, from the medium. To confirm that these trends are not dependent on the medium, we performed analogous experiments using Tris:TSB and observed that AAA and ΔHis_3Asp-AAA decreased Zn levels more readily than CP-Ser and ΔHis_3Asp, respectively (Figure S12; Tables S21–S37).

The Hexahistidine Motif Prevents Microbial Zn(II) Acquisition from Site 2

To evaluate whether these trends in Zn depletion correlated with antibacterial activity, we conducted growth studies of *L. plantarum* with CP variants. CP-Ser and AAA inhibited the growth of *L. plantarum* in Tris:MRS, whereas neither ΔHis_3Asp nor ΔHis_3Asp-AAA

exhibited antibacterial activity (Figure 7A). Despite the enhanced ability of the His_4 motif variants (AAA and ΔHis_3Asp-AAA) to deplete Zn from the medium compared to their His_6 analogues (CP-Ser and ΔHis_3Asp), the His_4 motif without the tail His residues does not appear to be sufficient to withhold Zn(II) from *L. plantarum*. This outcome is best exemplified by the fact that 250 μg/mL (≈11 μM heterodimer) ΔHis_3Asp-AAA reduced the Zn level in Tris:MRS from ≈ 10 to ≈ 1.5 μM, whereas full bacterial growth was observed with 1.0 mg/mL of this variant present in the medium. Residues His103 and His105 are not essential for high-affinity Zn(II) chelation at site 2; however, on the basis of these results, we concluded that the intact His_6 site is required for site 2 to sequester Zn(II) and thereby deprive microbes of this nutrient.

We therefore hypothesized that Zn(II) bound to CP at the His_6 site does not contribute to the bioavailable Zn(II) pool. To test this hypothesis and evaluate whether Zn(II) at site 2 of H103A, H105A, or AAA can be acquired by microorganisms, we cultured *L. plantarum* in low-Zn Tris:MRS (prepared by treating Tris:MRS with 250 μg/mL CP-Ser and removing the protein by spin filtration), added Zn(II)-bound CP-Ser or variant, and monitored bacterial growth over 20 h. *L, plantarum* grew to OD_{600} ≈ 0.6 in untreated Tris:MRS (≈10 μM Zn), and this value decreased to ≈ 0.2 in the low-Zn medium (≈1.5 μM Zn) (Figure 7B). When Zn(II)-bound CP-Ser, ΔHis_4, ΔHis_3Asp, or ΔHis_3Asp(H104A) was added to the culture, no growth recovery occurred. In contrast, growth recovery comparable to that of the +Zn(II) control was observed for cultures supplemented with Zn(II)-bound ΔHis_3Asp(H103A), ΔHis_3Asp(H105A), and ΔHis_3Asp-AAA. HPLC of the recovered culture supernatants revealed that both CP subunits remained intact (Figure S15). Thus, the growth recovery observed for the Zn(II)-bound tail variants does not result from Zn(II) release caused by protein degradation or instability. These assays indicate that the native His_6 motif is required for site 2 to sequester Zn(II) from *L. plantarum*. Despite the fact that CP variants with mutations in the tail retain the ability to coordinate Zn(II) with high affinity (Figure 5), the Zn(II) ion is sufficiently labile to be acquired by *L. plantarum* in the absence of S100A9 tail His residues.

To determine whether Zn(II) coordinated to CP tail variants is available to another microorganism, we extended this study to the opportunistic fungal pathogen *Candida albicans*. This fungus is susceptible to CP-mediated growth inhibition[38,39] and has a high metabolic Zn requirement,[40,41] and a number of Zn(II)-scavenging mechanisms have been implicated in the pathogenesis of *C. albicans*.[42–44] We therefore questioned whether *C. albicans* can acquire Zn(II) from site 2 of CP. In an analogous metal-supplementation assay, *C. albicans* was grown in Zn(II)-depleted medium (Tris:dYPD) (Tables S38–S39) in the absence and presence of a 7-μM Zn(II) supplement pre-incubated with CP variants, and the turbidity of the cultures was measured over a 24-h time course (Figure 7C). Consistent with the results from the *L. plantarum* growth study, Zn(II) bound to the native CP sites resulted in attenuated growth, and only maximal growth recovery (comparable to “free” Zn(II) addition) was observed when the His_6 motif was perturbed. In total, these growth studies support that the His_6 motif prevents microbial acquisition of this metal-ion nutrient and contributes to the growth inhibitory function of CP.

Summary and Perspective

In this work, we further evaluate the metal coordination chemistry and antimicrobial activity of CP and present the discovery that this host-defense protein employs its functionally multifaceted hexahistidine motif to coordinate Zn(II) and to sequester this essential nutrient from microbes, including an opportunistic fungal pathogen. This work expands the known coordination chemistry of biological Zn(II) sites and highlights additional facets to the remarkable bioinorganic chemistry of human CP. From the standpoint of host-defense function, CP is a versatile metal-sequestering protein that captures multiple first-row transition metal ions. Its behavior contrasts other metal-sequestering host-defense proteins such as lactoferrin and S100A12 (calgranulin C), which sequester specific nutrient metals (e.g. lactoferrin, Fe(III); S100A12, Zn(II)).[45–47] The unique hexahistidine site provides CP with its remarkable ability. Our spectroscopic analysis of Zn(II) at site 2 indicates that oxygen-donating ligands from water molecules do not have access to this metal ion, consistent with our prior investigations where we proposed a model highlighting the potential of the S100A9 C-terminal tail to encapsulate Mn(II) and Fe(II), allowing capture of kinetically labile metals at site 2.[10,17] Thus, we now extend this model to Zn(II) and reason that a similar coordination motif is employed when site 2 coordinates other first-row transition metals such as Co(II) and Ni(II).[10,13] Future investigations will address this notion and further evaluate the strategy of coordinative saturation and metal encapsulation to starve microbes of metal nutrients.

In early studies, CP was identified as an antifungal agent in neutrophil lysates[6] and was later shown to be associated with neutrophil extracellular traps (NETs).[39,48] Our findings indicate that CP effectively withholds Zn(II) from *C. albicans*. In contrast, a recent report demonstrated that the Gram-negative pathogen *Neisseria meningitidis* is able to acquire Zn(II) from CP by employing the zinc-pirating membrane protein CpbA.[49] The mechanism by which this bacterial protein scavenges Zn(II) from CP is currently unclear, and understanding the molecular details of metal exchange between host and pathogen chelators may help uncover strategies for targeting microbial systems of nutrient acquisition.

From the broader standpoints of physiology and metal homeostasis, CP is an abundant protein implicated in a variety of pathologies that include prostate disease, neurological disorders, and cancer.[50–55] We expect that future efforts will illuminate how CP contributes to the biology of Zn(II) beyond the host/microbe interaction.

Supplementary Material

Refer to Web version on PubMed Central for supplementary material.

Acknowledgments

We thank the NSF (CHE-1352132), the NIH (DP2OD007045), the Camille and Henry Dreyfus Foundation, and the Alfred P. Sloan Foundation for financial support. We thank Ms. Rose C. Hadley for technical assistance. T.G.N. is a recipient of the NSF Graduate Research Fellowship. The MIT Biophysical Instrumentation Facility for the Study of Complex Macromolecular Systems is supported by NSF-0070319. Zn K-edge X-ray absorption spectroscopy was performed at the Canadian Light Source, which is supported by the Canada Foundation for Innovation, Natural Sciences and Engineering Research Council of Canada, the University of Saskatchewan, the Government of

Saskatchewan, Western Economic Diversification Canada, the National Research Council Canada, and the Canadian Institutes of Health Research.

References

1. Vallee BL, Falchuk KH. Physiol Rev. 1993; 73:79–118. [PubMed: 8419966]
2. Kehl-Fie TE, Skaar EP. Curr Opin Chem Biol. 2010; 14:218–224. [PubMed: 20015678]
3. Hood MI, Skaar EP. Nat Rev Microbiol. 2012; 10:525–537. [PubMed: 22796883]
4. Diaz-Ochoa VE, Jellbauer S, Klaus S, Raffatellu M. Front Cell Infect Microbiol. 2014; 4:2. [PubMed: 24478990]
5. Cerasi M, Ammendola S, Battistoni A. Front Cell Infect Microbiol. 2013; 3:108. [PubMed: 24400228]
6. Sohnle PG, Collins-Lech C, Wiessner JH. J Infect Dis. 1991; 164:137–142. [PubMed: 2056200]
7. Clohessy PA, Golden BE. Scand J Immunol. 1995; 42:551–556. [PubMed: 7481561]
8. Loomans HJ, Hahn BL, Li QQ, Phadnis SH, Sohnle PG. J Infect Dis. 1998; 177:812–814. [PubMed: 9498472]
9. Corbin BD, Seeley EH, Raab A, Feldmann J, Miller MR, Torres VJ, Anderson KL, Dattilo BM, Dunman PM, Gerads R, Caprioli RM, Nacken W, Chazin WJ, Skaar EP. Science. 2008; 319:962–965. [PubMed: 18276893]
10. Nakashige TG, Zhang B, Krebs C, Nolan EM. Nat Chem Biol. 2015; 11:765–771. [PubMed: 26302479]
11. Korndörfer IP, Brueckner F, Skerra A. J Mol Biol. 2007; 370:887–898. [PubMed: 17553524]
12. Kehl-Fie, Thomas E, Chitayat S, Hood MI, Damo S, Restrepo N, Garcia C, Munro Kim A, Chazin Walter J, Skaar, Eric P. Cell Host Microbe. 2011; 10:158–164. [PubMed: 21843872]
13. Brophy MB, Hayden JA, Nolan EM. J Am Chem Soc. 2012; 134:18089–18100. [PubMed: 23082970]
14. Hayden JA, Brophy MB, Cunden LS, Nolan EM. J Am Chem Soc. 2013; 135:775–787. [PubMed: 23276281]
15. Damo SM, Kehl-Fie TE, Sugitani N, Holt ME, Rathi S, Murphy WJ, Zhang Y, Betz C, Hench L, Fritz G, Skaar EP, Chazin WJ. Proc Natl Acad Sci USA. 2013; 110:3841–3846. [PubMed: 23431180]
16. Brophy MB, Nakashige TG, Gaillard A, Nolan EM. J Am Chem Soc. 2013; 135:17804–17817. [PubMed: 24245608]
17. Gagnon DM, Brophy MB, Bowman SEJ, Stich TA, Drennan CL, Britt RD, Nolan EM. J Am Chem Soc. 2015; 137:3004–3016. [PubMed: 25597447]
18. Irving H, Williams RJP. J Chem Soc. 1953:3192–3210.
19. Clark-Baldwin K, Tierney DL, Govindaswamy N, Gruff ES, Kim C, Berg J, Koch SA, Penner-Hahn JE. J Am Chem Soc. 1998; 120:8401–8409.
20. Costello AL, Sharma NP, Yang KW, Crowder MW, Tierney DL. Biochemistry. 2006; 45:13650–13658. [PubMed: 17087519]
21. Brown ID, Altermatt D. Acta Crystallogr Sect B. 1985; 41:244–247.
22. Thorp HH. Inorg Chem. 1992; 31:1585–1588.
23. International Union of Crystallography. [accessed Jun 23, 2016] Bond Valence Parameters. http://www.iucr.org/resources/data/datasets/bond-valence-parameters
24. Berman HM, Westbrook J, Feng Z, Gilliland G, Bhat TN, Weissig H, Shindyalov IN, Bourne PE. Nucl Acids Res. 2000; 28:235–242. [PubMed: 10592235]
25. Groom CR, Bruno IJ, Lightfoot MP, Ward SC. Acta Cryst B. 2016; 72:171–179.
26. Garrett TPJ, Guss JM, Freeman HC. Acta Cryst C. 1983; 39:1027–1031.
27. Carballo R, Castiñeiras A, Covelo B, García-Martínez E, Niclós J, Vázquez-López EM. Polyhedron. 2004; 23:1505–1518.
28. Dudev T, Lim C. Chem Rev. 2003; 103:773–788. [PubMed: 12630852]

29. Sousa SF, Lopes AB, Fernandes PA, Ramos MJ. Dalton Trans. 2009:7946–7956. [PubMed: 19771357]
30. Silvennoinen L, Sandalova T, Schneider G. FEBS Lett. 2009; 583:2917–2921. [PubMed: 19665022]
31. Burdette SC, Frederickson CJ, Bu W, Lippard SJ. J Am Chem Soc. 2003; 125:1778–1787. [PubMed: 12580603]
32. Maret W, Vallee BL. Proc Natl Acad Sci USA. 1998; 95:3478–3482. [PubMed: 9520391]
33. Talmard C, Bouzan A, Faller P. Biochemistry. 2007; 46:13658–13666. [PubMed: 17983245]
34. Kwon JE, Lee S, You Y, Baek KH, Ohkubo K, Cho J, Fukuzumi S, Shin I, Park SY, Nam W. Inorg Chem. 2012; 51:8760–8774. [PubMed: 22534151]
35. Archibald FS, Duong MN. J Bacteriol. 1984; 158:1–8. [PubMed: 6715278]
36. Mrvčić J, Prebeg T, Barišić L, Stanzer D, Bačun-Družina V, Stehlik-Tomas V. Food Technol Biotechnol. 2009; 47
37. Leonardi A, Zanoni S, De Lucia M, Amaretti A, Raimondi S, Rossi M. ISRN Biotechnol. 2013; 2013:5.
38. Santhanagopalan V, Hahn BL, Sohnle PG. J Infect Dis. 1995; 171:1289–1294. [PubMed: 7751705]
39. Urban CF, Ermert D, Schmid M, Abu-Abed U, Goosmann C, Nacken W, Brinkmann V, Jungblut PR, Zychlinsky A. PLoS Pathog. 2009; 5:e1000639. [PubMed: 19876394]
40. Bedell GW, Soll DR. Infect Immun. 1979; 26:348–354. [PubMed: 387610]
41. Sabie FT, Gadd GM. Mycol Res. 1990; 94:952–958.
42. Wilson D. Metallomics. 2015; 7:979–985. [PubMed: 25652414]
43. Wilson D, Citiulo F, Hube B. PLoS Pathog. 2012; 8:e1003034. [PubMed: 23308062]
44. Jung WH. Mycobiology. 2015; 43:179–183. [PubMed: 26539032]
45. Singh PK, Parsek MR, Greenberg EP, Welsh MJ. Nature. 2002; 417:552–555. [PubMed: 12037568]
46. Haley KP, Delgado AG, Piazuelo MB, Mortensen BL, Correa P, Damo SM, Chazin WJ, Skaar EP, Gaddy JA. Infect Immun. 2015; 83:2944–2956. [PubMed: 25964473]
47. Cunden LS, Gaillard A, Nolan EM. Chem Sci. 2016; 7:1338–1348. [PubMed: 26913170]
48. Bianchi M, Niemiec MJ, Siler U, Urban CF, Reichenbach J. J Allergy Clin Immunol. 2011; 127:1243–1252.e1247. [PubMed: 21376380]
49. Stork M, Grijpstra J, Bos MP, Mañas Torres C, Devos N, Poolman JT, Chazin WJ, Tommassen J. PLoS Pathog. 2013; 9:e1003733. [PubMed: 24204275]
50. Yanamandra K, Alexeyev O, Zamotin V, Srivastava V, Shchukarev A, Brorsson AC, Tartaglia GG, Vogl T, Kayed R, Wingsle G, Olsson J, Dobson CM, Bergh A, Elgh F, Morozova-Roche LA. PLoS One. 2009; 4:e5562. [PubMed: 19440546]
51. Wan SG, Taccioli C, Jiang Y, Chen H, Smalley KJ, Huang K, Liu XP, Farber JL, Croce CM, Fong LYY. Int J Cancer. 2011; 129:331–345. [PubMed: 20857495]
52. Berg-Hansen P, Vandvik B, Fagerhol M, Holmøy T. J Neuroimmunol. 2009; 216:98–102. [PubMed: 19800696]
53. Nakatani Y, Yamazaki M, Chazin WJ, Yui S. Mediators Inflamm. 2005; 2005:280–292. [PubMed: 16258195]
54. Gustafsson D, Breimer LH, Isaksson HS, Nilsson TK. Scand J Clinic Lab Invest. 2012; 72:34–38.
55. Sampson B, Fagerhol MK, Sunderkötter C, Golden BE, Richmond P, Klein N, Kovar IZ, Beattie JH, Wolska-Kusnierz B, Saito Y, Roth J. Lancet. 2002; 360:1742–1745. [PubMed: 12480428]

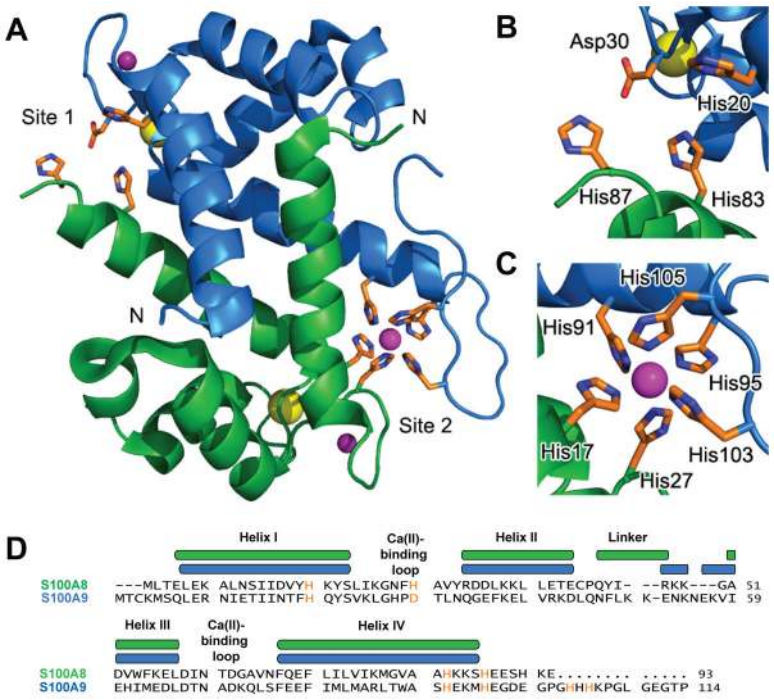

Figure 1.

CP has two transition-metal-binding sites at the S100A8/S100A9 dimer interface. (**A**) Crystal structure of Mn(II)-, Ca(II)- and Na(I)-bound CP-Ser (PDB: 4XJK).[17] The S100A8 subunit is shown in green. The S100A9 subunit is shown in blue. Na(I) ions are shown as purple spheres. Ca(II) ions are shown as yellow spheres. The Mn(II) ion is shown as a magenta sphere. (**B**) Site 1. (**C**) Site 2. (**D**) Amino acid sequence alignment of S100A8 and S100A9. The secondary structural elements are shown above the sequence. The transition metal-binding residues are shown in orange.

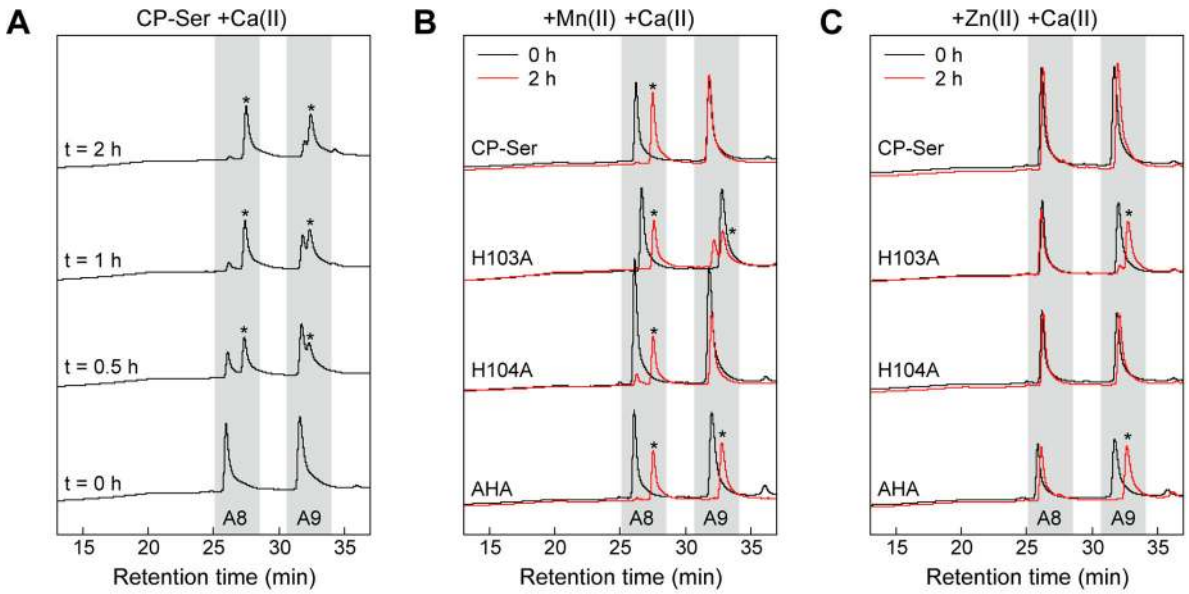

Figure 2.

Proteinase K digestion of CP-Ser and variants in the absence and presence of metal ions monitored by analytical HPLC (10–40% MeCN with 0.1% (v/v) trifluoroacetic acid (TFA) over 15 min followed by a gradient of 40–45% MeCN with 0.1% (v/v) TFA over 20 min at 1 mL/min 220 nm absorbance). (**A**) HPLC chromatograms of 30 μM CP-Ser incubated with 0.45 μM proteinase K in the presence of 1.5 mM Ca(II). (**B**) HPLC chromatograms of 30 μM CP-Ser and variants incubated with 0.45 μM proteinase K in the presence of 30 μM Mn(II) and 1.5 mM Ca(II). (**C**) HPLC chromatograms of 30 μM CP-Ser and variants incubated with 0.30 μM proteinase K in the presence of 60 μM Zn(II) and 1.5 mM Ca(II). In panels (**B**) and (**C**), the t = 0 h chromatogram is in black, and the t = 2 h chromatogram is in red. The gray regions denote peaks corresponding to the S100A8 and S100A9 subunits. Asterisks indicate the products of proteinase K cleavage.

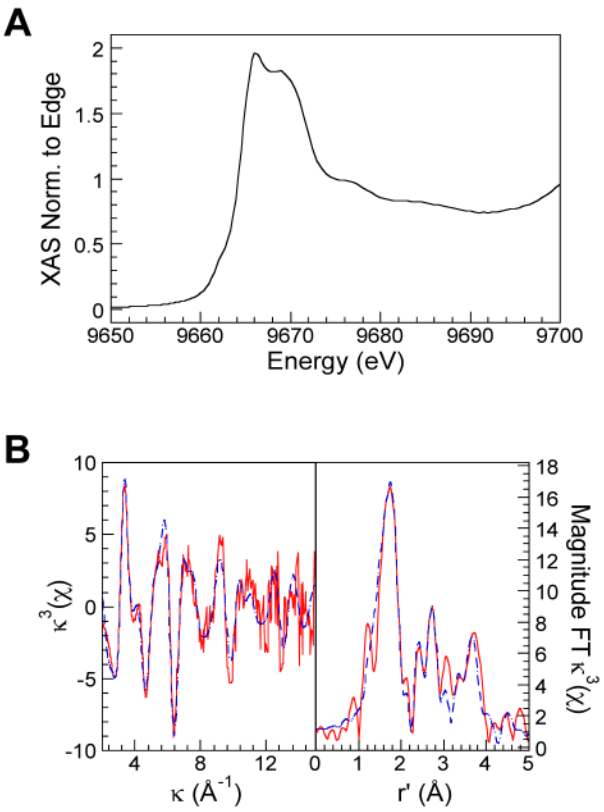

Figure 3.

X-ray absorption spectroscopy of Zn(II)-bound CP-Ser ΔHis_3Asp. (**A**) XANES region of the Zn K-edge X-ray absorption spectrum of Zn(II)-bound ΔHis_3Asp. (**B**) The $k^3(\chi)$ (left) and the magnitude Fourier Transformed (FT) $k^3(\chi)$ (right) spectra. Solid red spectra, experimental data; dashed blue spectra, simulated data. The displayed fit to the data is for the refinement with 4 longer Zn-N^{His} bonds and two shorter Zn-N^{His} bonds, which is visually virtually identical to the refinement with 3 longer and 3 shorter Zn-N^{His} bonds. The fits of the EXAFS spectra are given in Table S5.

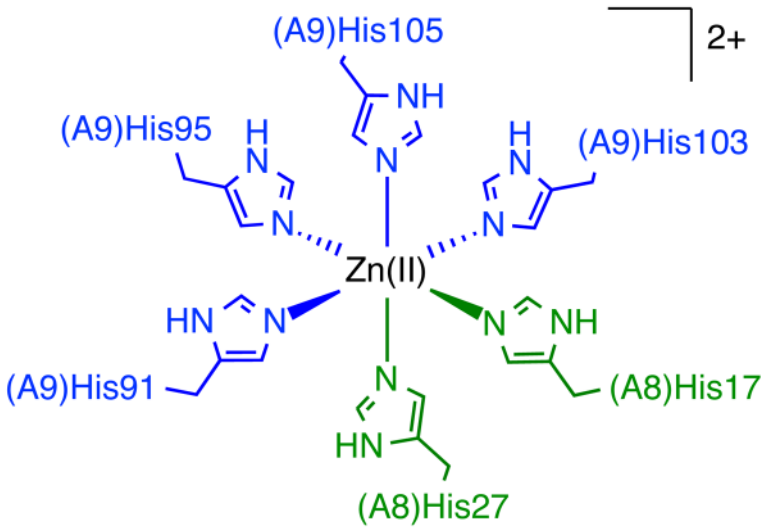

Figure 4.

The Zn(II)-His_6 coordination motif. Crystal structures of Mn(II)-bound CP-Ser show that the Nε atoms coordinate Mn(II),[15,17] and we propose the same occurs for Zn(II).

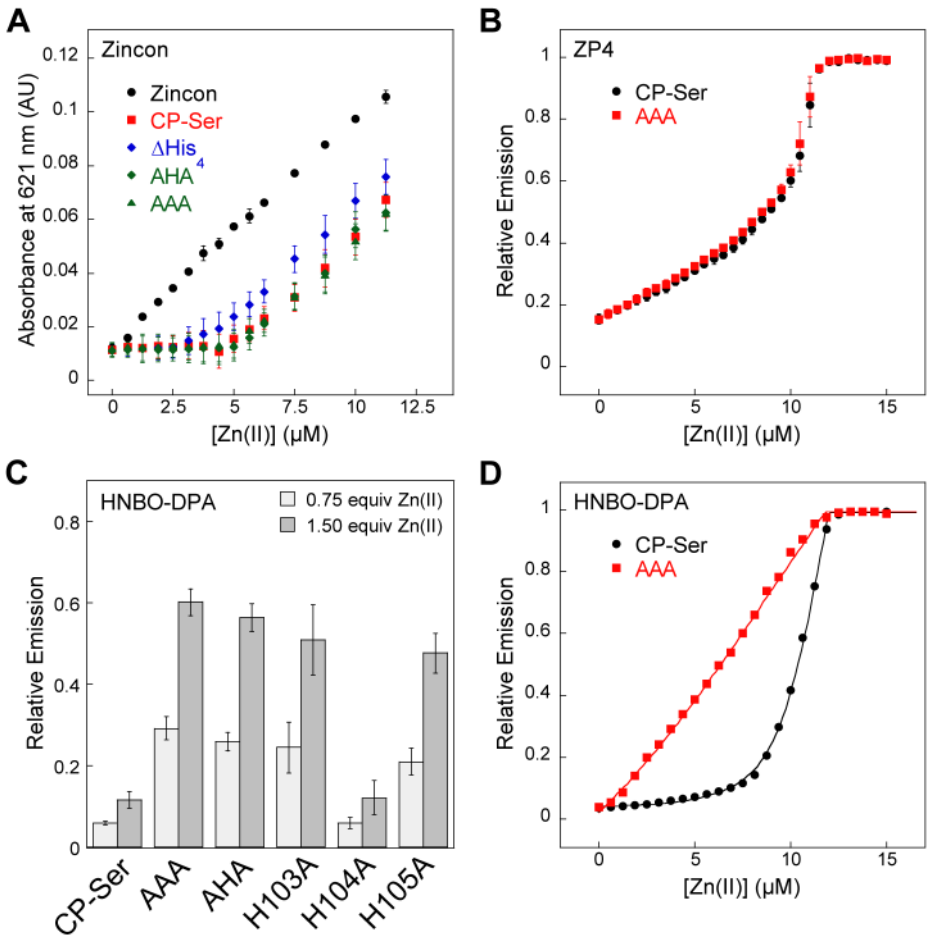

Figure 5.

Zn(II) competition with colorimetric and fluorescent probes. (**A**) Colorimetric response of 20 μM Zincon to Zn(II) with 2.5 μM CP variant and 250 μM Ca(II) in 75 mM HEPES, 100 mM NaCl, pH 7.0 at 25 ° C. Three independent titrations were performed for each sample, and the mean ± SDM are reported ($n = 3$). (**B**) Emission response of 2 μM ZP4 to Zn(II) in the presence of 5 μM CP and 250 μM Ca(II) in 75 mM HEPES, 100 mM NaCl, pH 7.0 at 25 °C. CP-Ser (black circles) and AAA (red squares) outcompete ZP4 for up to 2 equivalents Zn(II). The mean ± SDM are reported ($n = 3$). (**C**) Emission response of 2 mM HNBO-DPA with 5 μM CP-Ser, AAA, AHA, H103A, H104A, or H105A and 250 μM Ca(II) upon addition of 0.75 (light gray bars) and 1.50 equivalents of Zn(II) (dark gray bars) in 75 mM HEPES, 100 mM NaCl, pH 7.0 at 25 °C. Mean ± SDM are reported ($n = 3$). (**D**) Emission response of 2 μM HNBO-DPA to Zn(II) in the presence of 5 μM CP-Ser or AAA in 75 mM HEPES, 100 mM NaCl, 250 μM Ca(II), pH 7.0 at 25 °C. The mean values are reported ($n = 3$). The fits are shown as lines.

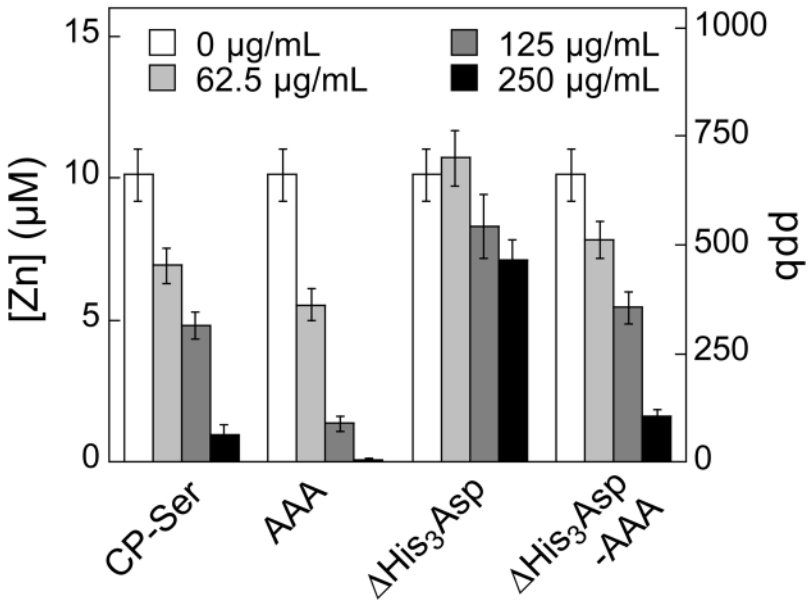

Figure 6.

Metal analysis of Tris:MRS (t = 20 h, 30 °C, 150 rpm) treated with CP variants (mean ± SEM, $n = 4$).

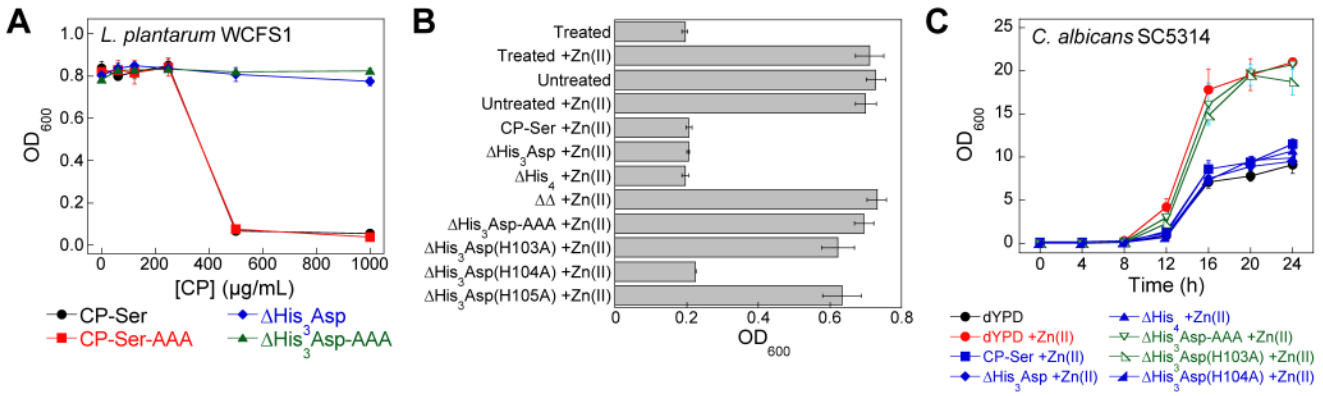

Figure 7.

CP sequesters Zn(II) from microbes employing the His_6 site. (**A**) Antimicrobial activity of CP-Ser and variants against *L. plantarum* (t = 20 h, 30 °C, 150 rpm) (mean ± SEM, $n = 3$). (**B**) *L. plantarum* growth in CP-treated or untreated medium in the absence or presence of a 10-μM Zn(II) supplement (t = 20 h, 30 °C, 150 rpm) (mean ± SEM, $n = 3$). (**C**) *C. albicans* growth in Zn(II)-depleted Tris:dYPD medium in the absence or presence of a 7-μM Zn(II) supplement (37 °C, 150 rpm) (mean ± SEM, $n = 3$).

Table 1

Nomenclature for Human Calprotectin Variants

Protein	S100A8 Mutation(s)	S100A9 Mutation(s)
CP	N/A	N/A
CP-Ser	C42S	C3S
CP-Ser ΔHis_3Asp	C42S, H83A, H87A	C3S, H20A, D30A
CP-Ser ΔHis_4	C42S, H17A, H27A	C3S, H91A, H95A
CP-Ser ΔΔ	C42S, H17A, H27A, H83A, H87A	C3S, H20A, D30A, H91A, H95A
CP-Ser(H103A)	C42S	C3S, H103A
CP-Ser(H104A)	C42S	C3S, H104A
CP-Ser(H105A)	C42S	C3S, H105A
CP-Ser-AHA	C42S	C3S, H103A, H105A
CP-Ser-AAA	C42S	C3S, H103A, H104A, H105A
CP-Ser ΔHis_3Asp(H103A)	C42S, H83A, H87A	C3S, H20A, D30A, H103A
CP-Ser ΔHis_3Asp(H104A)	C42S, H83A, H87A	C3S, H20A, D30A, H104A
CP-Ser ΔHis_3Asp(H105A)	C42S, H83A, H87A	C3S, H20A, D30A, H105A
CP-Ser ΔHis_3Asp-AAA	C42S, H83A, H87A	C3S, H20A, D30A, H103A, H104A, H105A